# Three-body collisions in Boltzmann-Uehling-Uhlenbeck theory*

A.B. Larionov[1,2,3], O. Buss[1], K. Gallmeister[1] and U. Mosel[1]

[1] *Institut für Theoretische Physik, Universität Giessen, D-35392 Giessen, Germany*

[2] *Frankfurt Institute for Advanced Studies,*

*J.W. Goethe-Universität, D-60438 Frankfurt am Main, Germany*

[3] *Russian Research Center Kurchatov Institute, 123182 Moscow, Russia*

(Dated: February 1, 2008)



## Abstract

Aiming at a microscopic description of heavy ion collisions in the beam energy region of about 10 A GeV, we extend the Giessen Boltzmann-Uehling-Uhlenbeck (GiBUU) transport model by including a relativistic mean field, in-medium baryon-baryon cross sections and three-body collisions. The model is then compared with experimental data for central Au+Au collisions at 2-10 A GeV and central Pb+Pb collisions at 30 and 40 A GeV on the proton rapidity spectra, the midrapidity yields of $\pi^+$, $K^\pm$ and $(\Lambda + \Sigma^0)$, and the transverse mass spectra of $\pi^\pm$ and $K^\pm$. The three-body collisions increase the inverse slope parameters of the hadron $m_\perp$-spectra to a good agreement with the data.

PACS numbers: 24.10.Lx; 24.10.Jv; 25.75.-q; 25.75.Dw

* Work supported by GSI Darmstadt

## I. INTRODUCTION

The Boltzmann-Uehling-Uhlenbeck (BUU) transport theory, based on binary collisions and on the propagation of particles in a selfconsistent mean field, is a very useful tool in understanding the heavy ion collisions (HIC) in the energy region from the Fermi energies ($E_{\rm lab} \sim 30$ A MeV) up to the relativistic energies ($E_{\rm lab} \sim 2$ A GeV) (c.f. Refs. [1, 2, 3, 4, 5, 6, 7] for the description of the model in various numerical realizations and Refs. [8, 9, 10, 11] for the results below 2 A GeV).

There are, however, systematic deviations from experimental data on pion and kaon production at $E_{\rm lab} > 2$ A GeV [12, 13, 14]: the pion multiplicity is systematically overpredicted, while the slopes of the $K^+$ transverse mass spectra are too steep in the transport calculations. It has been advocated in [13], that the too soft kaon $m_\perp$-spectra are caused by missing the formation of a nonhadronic phase, which should create an additional pressure accelerating the kaons. On the other hand, the three-fluid hydrodynamical calculations [15] have apparently been quite successfull in reproducing the $m_\perp$-spectra of hadrons at AGS to SPS energies by using a hadronic equation of state. This points to the idea of not enough thermalization produced by the microscopic transport models rather than to the importance of the nonhadronic degrees of freedom.

The many-body collisions — usually missed in the current transport calculations at high energies — could serve as an additional source of the thermalization. The role of many-body collisions grows with baryon density, which reaches values of order of 1-2 fm$^{-3}$ at the energy region of 10-20 A GeV [16]. These are typical energies of the future Compressed Baryonic Matter experiment at the Facility for Antiproton and Ion Research in Darmstadt [17].

A simple estimate of the gas parameter [18] at the baryon density $\rho_B = 10\rho_0$, which is the maximum density reached in a central Au+Au collision at 20 A GeV with $\rho_0 = 0.17$ fm$^{-3}$ being the normal nuclear matter density, is

$$\gamma_{\rm gas} = (\sigma/\pi)^{3/2}\rho_B \simeq 2 \ , \tag{1}$$

where $\sigma \simeq 40$ mb is the asymptotic high-energy value of the total pp cross section in vacuum. In thermally equilibrated nuclear matter, one can neglect the Lorentz contraction of the interaction volume $\frac{4}{3}\pi(\sigma/\pi)^{3/2}$ (c.f. Eqs.(A2),(46) and Fig. 2 below). Since $\gamma_{\rm gas} > 1$, one concludes, that the applicability condition of the binary collision approximation is violated

(c.f. Ref. [19]). As we have recently shown [20], at the maximum compression stage of the central Au+Au collision at 20 A GeV, $N$-body collisions with $N \geq 6$ should dominate.

One way to describe this complex physical situation could be, indeed, an introduction of the new degrees of freedom, e.g. like the formation of a quark-gluon plasma. This is quite a challenging problem for the microscopic transport theories, which is, however, beyond the scope of our present study. Another way is to simulate the many-body collisions within a theory containing only the hadronic degrees of freedom. At beam energies below 1-2 A GeV, transport models taking into account $N$-body collisions (with $N \geq 3$) have been constructed by several authors (c.f. Refs. [21, 22, 23, 24, 25]). The difficulty, which appears at high baryon densities reached in the 10 A GeV region is that the gas parameter is not small, and, therefore, such a theory can not be formulated with the vacuum cross sections as a decomposition of the collision integral in a series of powers of $\gamma_{\rm gas}$ (c.f. Ref. [18]). In other words, the vacuum cross sections should be screened at high densities by particles surrounding the colliding pair [26]. The screening effect appears also as a consequence of the Dirac-Brueckner calculations (c.f. Refs. [27, 28]), where the nuclear mean field and the in-medium reduced cross sections are derived from the same fundamental vacuum interaction. Using in-medium reduced cross sections would reduce the relative contribution of the many-body collisions, since the gas parameter will be smaller. This would give a more solid ground to the kinetic theory, which is based on the small parameter $\gamma_{\rm gas}$. The Fermi liquid theory [29, 30] gives a similar picture. There, the liquid of the real particles is equivalently replaced by the gas of quasiparticles.

In the present work, we develop a transport model which contains a Walecka-type baryonic mean field and the in-medium reduced baryon-baryon cross sections. The model is then extended by including three-body collisions. The mean field and the in-medium reduced cross sections lead to less thermalization, while the three-body collisions counterbalance this effect. We will show that the three-body collisions raise the inverse slope parameters of the hadron spectra in the central HIC at beam energies of 2-40 A GeV. In particular, the measured $K^+$ transverse mass spectra are well described by calculations with the three-body collisions.

The structure of the paper is as follows. In Sect. II we briefly describe the GiBUU model [7] concentrating on its new ingredients: the relativistic mean field, the in-medium baryon-baryon cross sections and the three-body collisions. Sect. III contains numerical results. In

Sect. IV we summarize and discuss our results.

## II. GIBUU MODEL

Our calculations are based on the GiBUU model in a new version of Ref. [7], written using FORTRAN 2003 in an object-oriented way. The model describes a nucleus-nucleus collision explicitly in time as a sequence of the baryon-baryon, meson-baryon and meson-meson collisions, baryon and meson resonance excitations and decays. Between the two-body collisions the particles propagate in a selfconsistent mean field. The baryon-baryon collisions at $\sqrt{s} \leq 2.6$ GeV are treated within the resonance model, while at $\sqrt{s} > 2.6$ GeV the FRITIOF model is applied. For the meson-baryon collisions, the FRITIOF model is used at $\sqrt{s} > 2.2$ GeV. We applied the energy-dependent strangeness suppression factor

$$\gamma_s \equiv \frac{P(s)}{P(u)} = \begin{cases} 0.4 & \text{for } \sqrt{s} \leq 5 \text{ GeV} \\ 0.433 - \frac{1}{150}\sqrt{s}\,[\text{GeV}]^{-1} & \text{for } 5 \text{ GeV} < \sqrt{s} < 20 \text{ GeV} \\ 0.3 & \text{for } \sqrt{s} \geq 20 \text{ GeV} \end{cases} \tag{2}$$

from Ref. [31] instead of the default FRITIOF value of $\gamma_s = 0.3$. In the meson-baryon collision case, the FRITIOF mechanism of the double-string excitation and decay has been improved by adding the $q\bar{q}$ annihilation channel as described in Ref. [14].

The particles produced in string decays are not allowed to interact with their default cross sections up to some proper time interval, called formation time. We use a value of the formation time $\tau_f = 0.8$ fm/c for all baryons and mesons. If one of the colliding particles is still in the formation interval, we call it a prehadron. The total cross section of the prehadron interaction with another particles is scaled according to the constituent quark model (c.f. Ref. [32]): If the prehadron interacts with a hadron, the total cross section is multiplied by the factor of $N_{\text{leading}}/3$ ($N_{\text{leading}}/2$) for the pre-baryon (pre-meson), where $N_{\text{leading}}$ is the number of leading (anti)quarks in the prehadron, i.e. the number of (anti)quarks which were existing in the parent colliding particles for the given prehadron. If both colliding particles are prehadrons, the total cross section of their interaction is multiplied by the product of the two corresponding factors.

The rescaling factor of the prehadron cross sections is quite important for the description of the produced particle multiplicities. In previous GiBUU calculations of HIC at 2-40 A GeV [14], this factor had been chosen to be 1/3 for the prehadrons containing at least one

leading quark and zero otherwise. This explains the higher particle abundancies produced in the cascade mode in the present paper as compared to the results of Ref. [14]. Another distinction to the calculations of Ref. [14] is that in the present work we miss the low energy ($\sqrt{s} \leq 2.6$ GeV) baryon-baryon channel of kaon production $BB \to BYK$. However, this channel was found to be negligible for the beam energies above 4 A GeV [14].

In this work, we improve the previous GiBUU calculations [14] by implementing a relativistic mean field (RMF), in-medium cross sections and three-body collisions in the model. The in-medium cross sections for the high energy baryon-baryon collisions computed according to the RMF model have already been introduced in [14]. However, the RMF has not been used for the particle propagation in [14]. Below, we describe in-detail these new ingredients of our model.

### A. Relativistic mean field

In distinction to the earlier GiBUU calculations [5, 6, 8, 9, 11, 32], where the nonrelativistic momentum-dependent potential of Ref. [33] was used, in the present work we employ the relativistic treatment of the baryonic mean field. In spite of the Lorentz invariant implementation of the potential from [33], when it is calculated in the local rest frame of nuclear matter, the RMF is better suited for description of the high baryon densities reached in a central heavy ion collision at about 10 A GeV beam energy. Here, a consistent nuclear equation of state at high densities is of the primary importance. RMF models provide a quite good description of both the collective flow in HIC and of the high density interior of neutron stars [34, 35]. They are also successfully applied in nuclear structure calculations [36]. The one weakness of the RMF models, the too repulsive nucleon-nucleus interaction at high momenta (c.f. [34] and refs. therein) , is of minor relevance for the present results for particle production from high-density equilibrated nuclear matter.

We use the relativistic mean field Lagrangian density in the form given in Ref. [36]:

$$\begin{aligned} \mathcal{L} &= \bar{\psi}[\gamma(i\partial - g_\omega\omega) - m_{\rm nuc} - g_\sigma\sigma]\psi \\ &+ \frac{1}{2}(\partial\sigma)^2 - U(\sigma) - \frac{1}{4}F_{\mu\nu}F^{\mu\nu} + \frac{1}{2}m_\omega^2\omega^2 \ , \end{aligned} \tag{3}$$

where $\psi$ is the nucleon field, $\sigma$ and $\omega$ are the scalar-isoscalar and the vector-isoscalar meson fields, respectively; $F_{\mu\nu} = \partial_\mu\omega_\nu - \partial_\nu\omega_\mu$. We neglect the isovector meson and the electromag-

netic contributions. The Lagrangian density (3) contains the nonlinear self-interactions of the $\sigma$-field:

$$U(\sigma) = \frac{1}{2}m_\sigma^2\sigma^2 + \frac{1}{3}g_2\sigma^3 + \frac{1}{4}g_3\sigma^4 \ . \tag{4}$$

The Lagrange's equations of motion for the nucleon, $\sigma$- and $\omega$-fields are written as follows:

$$[\gamma(i\partial - g_\omega\omega) - m_{\rm nuc} - g_\sigma\sigma]\psi = 0 \ , \tag{5}$$

$$\partial_\mu\partial^\mu\sigma + \frac{\partial U(\sigma)}{\partial\sigma} = -g_\sigma\bar{\psi}\psi \ , \tag{6}$$

$$\partial_\mu F^{\mu\nu} + m_\omega^2\omega^\nu = g_\omega\bar{\psi}\gamma^\nu\psi \ . \tag{7}$$

The $\sigma$- and $\omega$-fields are treated as classical ones, i.e. we replace these fields by their expectation values in Eqs.(5, 6, 7). Assuming that the meson fields are varying much more slowly in time and space with respect to the nucleon field, we consider the plane-wave solutions of Eq.(5):

$$\psi^{(\pm)} \propto \exp(\mp ipx) \ , \tag{8}$$

where $x \equiv (t, \mathbf{r})$, $p \equiv (p^0, \mathbf{p})$, and the upper (lower) sign corresponds to the nucleon (antinucleon). The dispersion relation is then obtained from (5):

$$p^0 = \pm g_\omega\omega^0 + \sqrt{(\mathbf{p} \mp g_\omega\boldsymbol{\omega}\ )^2 + (m_{\rm nuc}^\star)^2} \ , \tag{9}$$

where

$$m_{\rm nuc}^\star = m_{\rm nuc} + g_\sigma\sigma \tag{10}$$

is the nucleon effective (Dirac) mass.

The distribution function $f(x, \mathbf{p})$ of a given particle species in the phase space $(\mathbf{r}, \mathbf{p})$ is defined now such that $f(x, \mathbf{p})\frac{gd^3rd^3p}{(2\pi)^3}$ = (number of particles of that species in the phase space element $d^3rd^3p$), where $g = 4$ is the spin-isospin degeneracy. The space-time evolution of the (anti)nucleon phase space distribution function is described by the BUU equation

$$\frac{\partial f}{\partial t} + \frac{\partial p^0}{\partial \mathbf{p}}\frac{\partial f}{\partial \mathbf{r}} - \frac{\partial p^0}{\partial \mathbf{r}}\frac{\partial f}{\partial \mathbf{p}} = I_{\rm coll}[f] \ , \tag{11}$$

where — in spirit of the Fermi liquid theory [29, 30] — the single-particle energy (9) is used as a one-body Hamiltonian function. The l.h.s. of Eq.(11) describes the propagation of particles in the mean field, while the r.h.s. is the collision integral. The explicit form of $I_{\rm coll}$ for elastic scattering is given below (see Eqs.(15),(22),(A4)).

It is convenient to perform a variable transformation in Eq.(11) by using the kinetic four-momentum

$$p^{\star\mu} = p^\mu \mp g_\omega \omega^\mu \ . \tag{12}$$

The distribution function $f^\star(x, \mathbf{p}^\star)$ in the kinetic phase space $(\mathbf{r}, \mathbf{p}^\star)$ is defined such that $f^\star(x, \mathbf{p}^\star)\frac{g d^3r d^3p^\star}{(2\pi)^3}$ = (number of particles in the kinetic phase space element $d^3r d^3p^\star$). Since $d^3p = d^3p^\star$, which is valid for the momentum-independent $\omega$-field, one gets:

$$f^\star(x, \mathbf{p}^\star) = f(x, \mathbf{p}) \ . \tag{13}$$

Expressing the l.h.s. of Eq.(11) in terms of the kinetic quantities we obtain the transport equation (c.f. Ref. [34]):

$$(p_0^\star)^{-1}[p_\mu^\star \partial_x^\mu + (\pm g_\omega p_\nu^\star F^{\alpha\nu} + m_{\rm nuc}^\star(\partial_x^\alpha m_{\rm nuc}^\star))\partial_\alpha^{p^\star}] f^\star(x, \mathbf{p}^\star) = I_{\rm coll}[f^\star] \ , \tag{14}$$

where $\alpha = 1, 2, 3$, and $p_0^\star$ is determined from the mass shell condition $(p^\star)^2 = (m_{\rm nuc}^\star)^2$.

The collision integral, generally, can be expanded in the number of colliding particles (c.f. Ref. [22] and refs. therein):

$$I_{\rm coll}[f^\star] = I_{\rm coll,2b}[f^\star] + I_{\rm coll,3b}[f^\star] + I_{\rm coll,4b}[f^\star] + ... \ . \tag{15}$$

We will restrict ourselves to the first two terms in (15) only. It is straightforward to write down the elastic contributions to $I_{\rm coll,2b}$ and $I_{\rm coll,3b}$ in the case of identical fermions:

$$\begin{aligned} I^{\rm elastic}_{\rm coll,2b}[f_1^\star] = {} & \frac{1}{2!}\frac{m_1^\star}{p_1^{\star 0}} \int \frac{g d^3p_{1'}^\star m_{1'}^\star}{(2\pi)^3 p_{1'}^{\star 0}} \int \frac{g d^3p_{2'}^\star m_{2'}^\star}{(2\pi)^3 p_{2'}^{\star 0}} \int \frac{g d^3p_2^\star m_2^\star}{(2\pi)^3 p_2^{\star 0}} \\ & \times \overline{|M|^2_{12\to 1'2'}}\, (2\pi)^4\, \delta^{(4)}(p_1 + p_2 - p_{1'} - p_{2'})\, (f_{1'}^\star f_{2'}^\star \bar f_1^\star \bar f_2^\star - f_1^\star f_2^\star \bar f_{1'}^\star \bar f_{2'}^\star) \ , \end{aligned} \tag{16}$$

$$\begin{aligned} I^{\rm elastic}_{\rm coll,3b}[f_1^\star] = {} & \frac{1}{3!\,2!}\frac{m_1^\star}{p_1^{\star 0}} \int \frac{g d^3p_{1'}^\star m_{1'}^\star}{(2\pi)^3 p_{1'}^{\star 0}} \int \frac{g d^3p_{2'}^\star m_{2'}^\star}{(2\pi)^3 p_{2'}^{\star 0}} \int \frac{g d^3p_{3'}^\star m_{3'}^\star}{(2\pi)^3 p_{3'}^{\star 0}} \\ & \times \int \frac{g d^3p_2^\star m_2^\star}{(2\pi)^3 p_2^{\star 0}} \int \frac{g d^3p_3^\star m_3^\star}{(2\pi)^3 p_3^{\star 0}} \overline{|M|^2_{123\to 1'2'3'}} (2\pi)^4\, \delta^{(4)}(p_1 + p_2 + p_3 - p_{1'} - p_{2'} - p_{3'}) \\ & \times (f_{1'}^\star f_{2'}^\star f_{3'}^\star \bar f_1^\star \bar f_2^\star \bar f_3^\star - f_1^\star f_2^\star f_3^\star \bar f_{1'}^\star \bar f_{2'}^\star \bar f_{3'}^\star) \ , \end{aligned} \tag{17}$$

where $\overline{|M|^2_{12\to 1'2'}}$ and $\overline{|M|^2_{123\to 1'2'3'}}$ are the spin- and isospin-averaged over initial and final states matrix elements squared for two- and three-body collisions, respectively; $f_i^\star \equiv f^\star(x, \mathbf{p}_\mathbf{i}^\star)$, $\bar f_i^\star \equiv 1 - f_i^\star$ $(i = 1, 2, 3, 1', 2', 3')$. The matrix elements satisfy the detailed balance relations

$$\overline{|M|^2_{1'2'\to 12}} \ = \ \overline{|M|^2_{12\to 1'2'}} \ , \tag{18}$$

$$\overline{|M|^2_{1'2'3'\to 123}} \ = \ \overline{|M|^2_{123\to 1'2'3'}} \ , \tag{19}$$

which are used in Eqs.(16),(17). The normalization of Bjorken and Drell [37] is used for the matrix elements, which leads to the appearance of the fermion Dirac masses in Eqs. (16),(17). In the case of the momentum-independent $\sigma$-field used in this work, we have for the identical fermions $m_1^\star = m_2^\star = m_3^\star = m_{1'}^\star = m_{2'}^\star = m_{3'}^\star$. However, in Eqs.(16),(17) and everywhere below in the expressions for the collision integrals, we keep, for clarity, different subscripts for the Dirac masses of different particles.

Introducing the in-medium elastic differential scattering cross section

$$\begin{aligned} d\sigma^\star_{12\to 1'2'} &= (2\pi)^4\,\delta^{(4)}(p_1+p_2-p_{1'}-p_{2'})\,\overline{|M|^2_{12\to 1'2'}} \\ &\times \frac{m_1^\star m_2^\star}{I^\star_{12}}\,\frac{g d^3p^\star_{1'} m^\star_{1'}}{(2\pi)^3 p^{\star 0}_{1'}}\,\frac{g d^3p^\star_{2'} m^\star_{2'}}{(2\pi)^3 p^{\star 0}_{2'}}\,\frac{1}{2!} \end{aligned} \tag{20}$$

with

$$I^\star_{12} \equiv \sqrt{(p_1^\star p_2^\star)^2 - (m_1^\star m_2^\star)^2} \tag{21}$$

being the in-medium flux factor, one can rewrite the two-body elastic collision term as follows:

$$I^{\rm elastic}_{\rm coll,2b}[f_1^\star] = \int \frac{g d^3p_2^\star}{(2\pi)^3} \int d\sigma^\star_{12\to 1'2'}\, v^\star_{12} (f^\star_{1'} f^\star_{2'} \bar f^\star_1 \bar f^\star_2 - f^\star_1 f^\star_2 \bar f^\star_{1'} \bar f^\star_{2'}) \ , \tag{22}$$

where

$$v^\star_{12} = I^\star_{12}/(p_1^{\star 0} p_2^{\star 0}) \tag{23}$$

is the relative velocity of colliding particles.

In agreement with the low-energy in-medium calculations of the elastic NN scattering cross section (c.f. Ref. [38]), one can neglect the medium dependence of the matrix element $\overline{|M|^2_{12\to 1'2'}}$ approximately. This approximation will be used in the next subsection in order to evaluate the in-medium baryon-baryon cross sections (c.f. Eq.(35) below).

To solve Eq.(14), the distribution function in the kinetic phase space is projected onto test particles:

$$f^\star(x,\mathbf{p}^\star) = \frac{(2\pi)^3}{gN} \sum_{i=1}^{AN} \delta(\mathbf{r}-\mathbf{r_i}(t))\delta(\mathbf{p}^\star - \mathbf{p_i^\star}(t)) \ , \tag{24}$$

where $A$ is the number of nucleons and $N$ is the number of test particles per nucleon. The centroids of the $\delta$-functions are evolving in time between the two- or three-body collisions according to the following equations, which can be obtained by substituting (24) into (14) and putting the collision term equal to zero (c.f. Refs. [34, 39]):

$$\frac{d\mathbf{r}_i}{dt} = \frac{\mathbf{p}_i^\star}{p_i^{\star 0}} \ , \tag{25}$$

$$\frac{dp_i^{\star\alpha}}{dt} = \pm g_\omega \frac{p^\star_{i\nu}}{p_i^{\star 0}} F^{\alpha\nu} + \frac{m^\star_{\rm nuc}}{p_i^{\star 0}} \partial_x^\alpha m^\star_{\rm nuc} \tag{26}$$

with $\alpha = 1, 2, 3$ and $\nu = 0, 1, 2, 3$.

The $\sigma$- and $\omega$-fields are calculated from the Klein-Gordon equations (6),(7) by neglecting the derivatives of the fields in space and time:

$$m_\sigma^2 \sigma + g_2 \sigma^2 + g_3 \sigma^3 = -g_\sigma \rho_s \ , \tag{27}$$

$$m_\omega^2 \omega^\nu = g_\omega j_B^\nu \ . \tag{28}$$

$$\tag{29}$$

The scalar density $\rho_s(x) = < \bar{\psi}(x)\psi(x) >$ and the baryon current $j_B^\nu(x) = < \bar{\psi}(x)\gamma^\nu\psi(x) >$ are expressed via the (anti)nucleon phase space distribution functions:

$$\rho_s(x) \ = \ \int \frac{g d^3p^\star m^\star_{\rm nuc}}{(2\pi)^3 p^{\star 0}} (f^\star_{\rm nucleon}(x, \mathbf{p}^\star) + f^\star_{\rm antinucleon}(x, \mathbf{p}^\star)) \ , \tag{30}$$

$$j_B^\nu(x) \ = \ \int \frac{g d^3p^\star p^{\star\nu}}{(2\pi)^3 p^{\star 0}} (f^\star_{\rm nucleon}(x, \mathbf{p}^\star) - f^\star_{\rm antinucleon}(x, \mathbf{p}^\star)) \ . \tag{31}$$

Since we use the distribution functions in the kinetic phase space, Eqs.(27),(30) do not depend explicitly on the vector field $\omega$. This simplifies the selfconsistent numerical calculation of the meson mean fields strongly.

We assume, for simplicity, the same coupling constants of all other baryons with the $\sigma$- and $\omega$-fields as for the nucleon. Correspondingly, in actual calculations of the scalar density and of the baryon current, the partial contributions from all the baryons present in the system are taken into account. The baryon test particles are propagated according to Eqs.(25), (26) with a replacement $m^\star_{\rm nuc} \to m^\star_B = m_B + g_\sigma \sigma$, where $m_B$ is the vacuum mass of the baryon $B$. The potentials acting on mesons are neglected. Thus, the mesons are propagated freely between the two- or three-body collisions.

The numerical values of the RMF parameters were chosen according to the parameter set NL2 from Ref. [39]: $m_\sigma = 550.5$ MeV, $m_\omega = 783.3$ MeV, $g_\sigma = 8.50$, $g_\omega = 7.54$, $g_2 = -50.37$ fm$^{-1}$, $g_3 = -6.26$. This parameter set [40] produces the incompressibility $K = 210$ MeV and the ratio $m^\star_{\rm nuc}/m_{\rm nuc} = 0.83$ at normal nuclear matter density. At high densities, the NL2 parameter set gives a rather soft equation of state [34]. This agrees with the BEVALAC data on collective flow in HIC at about 1 A GeV beam energy [34].

The $\sigma$-field and the baryon four-current have been computed on the space grid with the cell sizes $\simeq (1 \times 1 \times 1/\gamma)$ fm covering the collision zone. The smaller cell size in the

longitudinal direction is needed in order to resolve the density profiles of the colliding nuclei, which are Lorentz contracted by the $\gamma$-factor in the center-of-mass (c.m.) frame. We have used the parallel ensemble technique (c.f. Ref. [1]) with $N = 200$ test particles per nucleon. To get smooth meson mean fields, the $\delta$-function in coordinate space $\delta(\mathbf{r} - \mathbf{r_i}(t))$ in Eq. (24) has been replaced by the Lorentz contracted gaussian

$$\rho_i(\mathbf{r}) = \frac{\gamma}{(2\pi)^{3/2} L^3} \exp\left\{ -\frac{(x - x_i(t))^2}{2L^2} - \frac{(y - y_i(t))^2}{2L^2} - \frac{(z - z_i(t))^2 \gamma^2}{2L^2} \right\} \tag{32}$$

with $L \simeq 1$ fm. The equations of motion (25),(26) for the test particles have been solved by using the $O(\Delta t^2)$ predictor-corrector method. The space derivatives in the r.h.s. of Eq.(26) have been computed using the central differences, which produces a second order accuracy also in space. The numerical scheme conserves energy with an accuracy better than 3% of the c.m. kinetic energy for the studied reactions.

### B. In-medium cross sections

The most important part of the GiBUU model is the collision integral which includes the hadron-hadron cross sections. In the case of cascade calculation, neglecting any mean field effects, the vacuum cross sections are invoked. These cross sections are based either on the resonance model or on the phenomenological parameterizations of the experimental data with some reasonable extrapolations to the not-measurable channels (e.g. in the case of meson-meson collisions). The detailed description of the low energy resonance cross sections is given in Refs. [3, 5, 6]. The high energy cross section parameterizations — used for the FRITIOF event generator — are explained in Ref. [32]. For the meson-meson cross sections, we refer the reader to Ref. [14].

Using the RMF model in particle propagation requires also to introduce in-medium modifications of the cross sections. This should be already clear, since the particle production thresholds include now the Dirac masses instead of the vacuum masses. To evaluate the cross sections in the case of calculations with RMF, we will apply two different schemes.

In the first scheme, a so-called corrected invariant energy of the two colliding particles 1 and 2 is computed as

$$\sqrt{s_{\rm corr}} = \sqrt{s^\star} - (m_1^\star - m_1) - (m_2^\star - m_2) \ , \tag{33}$$

where

$$s^\star = (p_1^\star + p_2^\star)^2 \ . \tag{34}$$

The corrected invariant energy is an analog of the vacuum invariant energy, since the scalar selfenergies of the colliding particles are subtracted in the r.h.s. of Eq.(33). The quantity $\sqrt{s_{\rm corr}}$ is then used in calculation of any reaction cross section $\sigma_{12\to X}(\sqrt{s_{\rm corr}})$. Due to the same scalar selfenergies for all the baryons, this scheme ensures the correct threshold conditions for all binary processes except for $B\bar{B}$ production/annihilation. The last processes are, however, not important at the beam energies considered in the present work.

In the second scheme, we follow the approach of Ref. [14]. There the in-medium cross section of a process $B_1B_2 \to B_3B_4M_5M_6...M_N$ with $B_{1,2}$ and $B_{3,4}$ as incoming and outgoing baryons and $M_{5,...,N}$ as produced mesons, is expressed in a form:

$$\sigma^{med}(\sqrt{s^\star}) = F\sigma^{vac}(\sqrt{s_{\rm corr}}) \ . \tag{35}$$

The modification factor $F$ is

$$F \equiv \frac{m_1^\star m_2^\star m_3^\star m_4^\star}{m_1m_2m_3m_4}\frac{I}{I^\star}\frac{\Phi_{N-2}(\sqrt{s^\star}; m_3^\star, m_4^\star, ..., m_N^\star)}{\Phi_{N-2}(\sqrt{s_{\rm corr}}; m_3, m_4, ..., m_N)} \ , \tag{36}$$

where

$$\Phi_n(M; m_1, m_2, ..., m_n) = \int d\Phi_n(P; p_1, p_2, ..., p_n) \tag{37}$$

is the $n$-body phase space volume with $m_i^2 = p_i^2$ $(i = 1, 2, ..., n)$ and $M^2 = P^2$,

$$d\Phi_n(P; p_1, p_2, ..., p_n) = \delta^{(4)}(P - p_1 - p_2 - ... - p_n)\frac{d^3p_1}{(2\pi)^3 2p_1^0}\frac{d^3p_2}{(2\pi)^3 2p_2^0}\cdots\frac{d^3p_n}{(2\pi)^3 2p_n^0} \tag{38}$$

is the element of the $n$-body phase space volume (c.f. Ref. [41]);

$$I_{12} \ = \ q(\sqrt{s_{\rm corr}}, m_1, m_2)\sqrt{s_{\rm corr}} \ , \tag{39}$$

$$I_{12}^\star \ = \ q(\sqrt{s^\star}, m_1^\star, m_2^\star)\sqrt{s^\star} \tag{40}$$

are the vacuum and in-medium flux factors (c.f. Eq.(21)) with

$$q(\sqrt{s}, m_1, m_2) = \sqrt{(s + m_1^2 - m_2^2)^2/(4s) - m_1^2} \tag{41}$$

being the center-of-mass (c.m.) momentum. Eqs.(35),(36) take into account the in-medium modification of the Dirac plane wave normalization (a factor of $m_1^\star m_2^\star m_3^\star m_4^\star/(m_1m_2m_3m_4)$), of the flux factor and of the phase space volume. However, it is assumed that the matrix

element of the reaction is not in-medium modified. Due to the Dirac mass reduction with the baryon density, the in-medium baryon-baryon cross section is substantially reduced in nuclear medium. In the present work, we have extended the method of Ref. [14] by applying Eqs.(35),(36) also for the in-medium modification of the channel $B_1B_2 \to B_3B_4$, i.e. for the elastic baryon-baryon collisions or resonance excitation in baryon-baryon collisions without outgoing mesons.

Meson-baryon cross sections were kept always as the vacuum ones. We believe that this is a reasonable assumption, since the modification factor will be proportional to $(m^\star)^2$ in this case, while the modification factor for the baryon-baryon cross sections is proportional to $(m^\star)^4$ (c.f. Eq.(36)). Thus, the meson-baryon cross sections are less subject to the in-medium modifications. On the other hand, the implementation of the in-medium meson-baryon cross sections is more difficult, since in this case also the resonance decay widths should be consistently modified to preserve detailed balance in the channel $MB \leftrightarrow R$.

For brevity, the first scheme will be refered to as the calculation with vacuum cross sections below. The second scheme will be called the calculation with the in-medium cross sections.

### C. Three-body collisions

Little is known about the three-body forces even in ground state nuclear matter. The problem of particle production in three-body collisions is even harder. There are no experimental data on this subject and the corresponding matrix elements are not obtainable from data [42]. Thus, in simulating the three-body collisions, we apply a simple geometrical method similar to that of Refs. [19, 22, 23, 24]. For the details of derivation we refer the reader to Ref. [24].

The geometrical method of Refs. [19, 22, 23, 24] is based on the hard-sphere collision picture, i.e. the potential acting between colliding nucleons 1 and 2 is assumed to be infinitely repulsive at relative distances $d_{12} \leq R_{\rm max}$ and zero at $d_{12} > R_{\rm max}$, where $R_{\rm max}$ is equal to the sum of the matter radii of the colliding particles. The quantity $R_{\rm max}$ can be expressed in terms of the total (in-medium) interaction cross section $\sigma^\star_{12}$ of the particles 1 and 2 as follows:

$$R_{\rm max} = \sqrt{\sigma^\star_{12}/\pi} \ . \tag{42}$$

The three-body collision is assumed to happen, if (i) the two nucleons 1 and 2 are about to collide according to the geometrical collision criterion [1] and (ii) the third particle is found in a sphere of radius $R_{\rm max}$ centered at the collision point of 1 and 2. The geometrical collision criterion for selecting the colliding pair 1 and 2 means that these particles approach their minimum separation distance during the given time step, and this distance is less than $R_{\rm max}$. Thus, the three-body collision takes place when all the three particles are found simultaneously in the interaction volume which is here the sphere of radius $R_{\rm max}$ centered at the c.m. of 1 and 2 in coordinate space.

The hard-sphere collision picture reflects, in a natural way, the short-range character of the nuclear forces acting between hadrons. However, in a high-energy nucleus-nucleus collision case, one must modify this picture to account for the Lorentz contraction of the matter radii of the colliding hadrons. The relativistic gas of the Lorentz-contracted hard spheres in thermal equilibrium has been already considered in Refs. [43, 44] in order to derive the Lorentz corrections to the excluded volume in the Van-der-Waalls equation of state.

Therefore, in the present work we define the interaction volume as an axially symmetric ellipsoid contracted along the collision axis of 1 and 2 by the average $\gamma$-factor in their c.m. frame

$$\gamma_{12} = ((\gamma_1 + \gamma_2)/2)_{\rm cm12} \ , \tag{43}$$

where $\gamma_1 = p_1^{\star 0}/m_1^\star$ and $\gamma_2 = p_2^{\star 0}/m_2^\star$. The ellipsoid has a half-axis of $R_{\rm max}/\gamma_{12}$ along the particle 1 momentum in the c.m. frame of 1 and 2 and a half-axis of $R_{\rm max}$ in a transverse direction.

We now select the set of all particles inside the ellipsoid which are different from 1 and 2. In principle, all the particles from the set plus the colliding pair form a many-body colliding system. However, for technical reasons, we restricted ourselves in this work to a simulation of three-body collisions only. Therefore, we choose only one particle from the set, namely, the closest particle to the c.m. of 1 and 2 — as a participant of a three-body collision. We will denote this particle as 3 below.

Next we simulate the actual three-body collision event of the triple 1, 2 and 3. We denote the initial kinetic momenta of the triple as $\mathbf{p_1^\star}$, $\mathbf{p_2^\star}$ and $\mathbf{p_3^\star}$. Following Ref. [22], the momenta of the triple are, first, redistributed microcanonically. This is done by sampling the new

kinetic momenta $\mathbf{p_{1'}^\star}$, $\mathbf{p_{2'}^\star}$ and $\mathbf{p_{3'}^\star}$ according to the probability

$$d\mathcal{P} \propto d\Phi_3(p_1^\star + p_2^\star + p_3^\star;\, p_{1'}^\star,\, p_{2'}^\star,\, p_{3'}^\star)\ , \tag{44}$$

where $d\Phi_3$ is the three-body phase space volume element (Eq.(38)). It is assumed here that the particles 1,2 and 3 keep their identity. In particular, they stay on their initial Dirac mass shells: $(p_{i'}^\star)^2 = (p_i^\star)^2 = (m_i^\star)^2$, i=1,2,3.

After the redistribution of the momenta, the two-body collision of the particles 1 and 2 with four-momenta $p_{1'}^\star$ and $p_{2'}^\star$ is simulated in a usual way. This can lead to either elastic or inelastic scattering, including multiple particle production through the FRITIOF mechanism. In Appendix A, the formal expressions for the three-body collision integral and the corresponding matrix element squared are given which reflects the procedure discussed above in the case of elastic collisions of identical fermions.

In the actual numerical simulations, we performed the search for the third particle, which can be either a baryon or a meson, only if the particles 1 and 2 are both baryons or a meson and a baryon. For the meson-meson collisions, the search for the third particle has not been done. The meson-meson collisions are, however, relatively soft and can not influence much the high-$p_t$ part of the spectra, which are of the primary interest in our present study.

To save the CPU time, we have also switched-off the Pauli blocking of the final state in all collision and resonance decay processes. We have checked by direct calculation, that above $E_{\rm lab} = 2$ A GeV the Pauli blocking is negligibly small.

## III. NUMERICAL RESULTS

We have performed the calculations for central Au+Au collisions at beam energies of 2-20 A GeV and central Pb+Pb collisions at 30 and 40 A GeV. The time evolution of the systems in the c.m. frame of the colliding nuclei has been followed up to 30 fm/c using a variable time step. The size of the time step was adjusted to reduce the spurious effect of multiple scatterings of the same particle within the given time step.

In order to see an influence of the various physical ingredients of our model, four types of calculation have been done: (i) pure binary cascade calculation without mean field and using the vacuum cross sections; (ii) the calculation with the RMF, with only binary collisions and vacuum cross sections; (iii) the same as (ii) plus the three-body collisions; (iv) the same

as (iii), but with the in-medium baryon-baryon cross sections.

It is necessary to point out, that when calculating the radius $R_{\max}$ of Eq.(42) we have used the cross section $\sigma_{12}^{\star}$ somewhat different from the actual total two-body cross section implemented in the model. Namely, in calculations with vacuum cross sections (i),(ii) and (iii), $\sigma_{12}^{\star}$ was set to 40 mb for a baryon-baryon collision, which is an asymptotic high energy value of the total $pp$ cross section. In the case of the calculation with in-medium baryon-baryon cross sections (iv), we used for $\sigma_{12}^{\star}$ the in-medium $pp$ cross section determined by summation of all possible final state channels. The in-medium cross section of each final channel was obtained according to Eq.(35). For the meson-baryon collisions, the constant cross section $\sigma_{12}^{\star} = 20$ mb was always used in Eq.(42). This value is close to the asymptotic high energy $\pi^+ p$ total cross section. The rescaling factors due to the leading quark numbers (c.f. Sect. II) have not been taken into account in the calculation of the interaction volume. To avoid misunderstanding, we stress that these simplifying assumptions have been made when calculating the interaction volume only, but not in determination of the two-body collision partners by the geometrical collision criterion.

### A. Time evolution

Fig. 1 shows the time dependencies of the central baryon and meson densities and of the total collision frequency for the Au+Au system at 20 A GeV and b=0 fm. The baryon and meson densities have been computed in the central 1fm×1fm×1fm cube. The total collision frequency $N_{\rm tot}$ includes the two- and (when switched-on) the three-body collisions and has been determined in the larger 3fm×3fm×3fm central cube to reduce the statistical fluctuations. The quantity $N_{\rm tot}$ reaches its maximum at about 4 fm/c, when also the central baryon and meson densities are maximal, and drops rapidly later on. We observe, that the RMF reduces the maximum baryon and meson densities and also leads to a faster expansion of the compressed system. The three-body collisions do not influence the central densities and influence the total collision frequency only weakly. The weakness of the dependence of the total collision frequency on the three-body collisions is due to the fact, that the inclusion of the three-body collisions reduces the number of the pure two-body collisions, i.e. collisions where there is no other particles in the interaction volume of the primary colliding pair 1 and 2. Indeed only about 10-20% of all collision events are now pure two-body (c.f. Fig. 2

below).

It is interesting, that the inclusion of three-body collisions even reduces $N_{\rm tot}$ slightly. This happens, since the particle $3'$ and the particles emerging from the interaction of $1'$ and $2'$ are final state particles of a three-body collision event (see Sect. IIC). The final state particles are not allowed to rescatter on each other before at least one of them will rescatter on another particle. This leads to an overall reduction of the total collision frequency, when the three-body collisions are included. Indeed, without the three-body collisions, the particle 3 would be allowed to rescatter on the collision products of 1 and 2.

Finally, using the in-medium baryon-baryon cross sections influences the baryon density rather weakly. However, the meson production and the total collision frequency are strongly decreased in this case.

Fig. 2 presents the ratio of the frequency of three-body collisions to the total collision frequency (two- plus three-body) as a function of time for the Au+Au central collision at 20 A GeV (bottom left and right panels). In order to understand this ratio better, we also show in Fig. 2 the time dependencies of the central baryon and meson densities along with their sum and the average $\gamma$-factor of the two-body collisions (top left and right panels). The cross section $\sigma^\star_{12}$ used to compute the radius $R_{\rm max}$ of Eq.(42) averaged over colliding pairs is also plotted vs time in Fig. 2 (middle left and right panels). Calculations both with vacuum (left column) and in-medium (right column) cross sections are shown in Fig. 2. We see that the ratio $N_3/N_{\rm tot}$ reaches the maximum value of 0.9 for the vacuum cross sections and 0.8 for the in-medium cross sections.

The ratio $N_3/N_{\rm tot}$ can be estimated on the basis of the Poissonian distribution for the probability to find $n = 0, 1, 2, ...$ particles in the interaction volume of the colliding pair 1 and 2 (c.f. Ref. [20]):

$$P_n = \frac{\lambda^n}{n!} \exp(-\lambda) \ , \tag{45}$$

where $\lambda = \rho_{\rm tot} < V_{12} >$ with $< V_{12} >$ being the averaged interaction volume (c.f. Eq.(A2)):

$$< V_{12} > \equiv \frac{4}{3}\pi \left( \frac{< \sigma^\star_{12} >}{\pi} \right)^{3/2} < \gamma_{12} >^{-1} \ . \tag{46}$$

For the meson-free matter, the quantity $\lambda$ is proportional to the gas parameter (Eq.(1)). Since, by definition (see Sect. IIC), the three-body collision happens if $n \geq 1$, the following estimate can be done:

$$N_3/N_{\rm tot} \simeq 1 - P_0 = 1 - \exp(-\lambda) \ . \tag{47}$$

In the nonrelativistic limit for the meson-free matter with $\lambda \ll 1$, Eq.(47) is identical to the result of Ref. [19]. The estimate (47) is depicted by the dashed lines in the bottom left and right panels of Fig. 2. We observe, that Eq.(47) reproduces the overall behaviour of the directly computed ratio $N_3/N_{\rm tot}$. In particular, one can see, that the flat maximum of $N_3/N_{\rm tot}$ calculated with the vacuum cross sections is caused by larger $< \sigma^\star_{12} >$ at the initial stage of collision. In the case of the in-medium baryon-baryon cross sections, the value of $< \sigma^\star_{12} >$ drops quickly at the beginning, reaching the minimum at about 2 fm/c. This reduces the ratio $N_3/N_{\rm tot}$ at the initial stage of the collision and leads to the peak of the ratio at about 5 fm/c. At $t > 10$ fm/c, the meson-nucleon collisions dominate. Thus, $< \sigma^\star_{12} >$ is close to 20 mb in both calculations, with vacuum and in-medium baryon-baryon cross sections. As a consequence, at $t > 10$ fm/c the ratio $N_3/N_{\rm tot}$, practically, does not depend on the baryon-baryon cross sections.

Another interesting feature is that the average $\gamma$-factor (c.f. dotted lines in the top left and right panels of Fig. 2) drops from initial value of 3.6 to a rather low value of 1.5 within 5 fm/c. This reflects the transition of the fast relative motion of colliding nuclei to a slower thermal motion of nearly equilibrated hadronic matter. The Lorentz contraction of the interaction volume (Eqs. (A2) and (46)) plays only a moderate role for the equilibrated hadronic medium. However, at the initial nonequilibrium stage, the Lorentz contraction suppresses the ratio $N_3/N_{\rm tot}$ very strongly. Thus, as it should be, the very early stage of a relativistic heavy ion collision can be described by the binary cascade model quite well.

Fig. 3 shows the beam energy dependence of the maximum central baryon and total densities and of the maximum ratio $N_3/N_{\rm tot}$ reached in central Au+Au collisions. RMF reduces the maximum baryon and total densities quite substantially (c.f. also Fig. 1). The three-body collisions do not influence these two observables. In calculation with the vacuum baryon-baryon cross sections, the ratio $N_3/N_{\rm tot}$ stays almost constant $\sim 0.9$ in the beam energy range from 2 to 20 A GeV. Using the in-medium baryon-baryon cross sections leads to a dropping $N_3/N_{\rm tot}$ towards smaller beam energies. Indeed, at smaller $E_{\rm lab}$, the in-medium reduction of the baryon-baryon cross sections is better visible, due to the smaller number of the meson-baryon collisions.

### B. Comparison with experiment

First, we address the stopping power of nuclear matter. Fig. 4 shows the proton rapidity distributions for the central Au+Au collisions at 10.7 A GeV (upper panel) and for the central Pb+Pb collisions at 40 A GeV (lower panel). The cascade calculation (i) clearly produces too much stopping. The same efect has also been observed in earlier GiBUU calculations [14].

Including the RMF reduces the stopping power. This brings the calculation (ii) into closer agreement with the midrapidity proton yields. It is interesting, that, at 40 A GeV, the proton rapidity distribution even develops a minimum at $y = 0$ indicating an onset of the transparency. Taking into account three-body collisions (iii) increases the stopping power strongly, which again results in an overestimation of the midrapidity proton yields. Ultimately, using in-medium cross sections (iv) reduces the stopping power in a good agreement with the data.

The in-medium reduced baryon-baryon cross sections reduce the stopping power due to less thermalization, while the three-body collisions act in the opposite direction leading to more thermalization. Indeed, a third particle found in the vicinity of the colliding pair interchanges its energy and momentum with the pair: we simulated this effect by micro-canonical sampling of the three-body phase space (c.f. Eq.(44). As a result, the relative momentum of the two colliding particles changes its direction according to the isotropic distribution. Therefore, the outgoing particles are also produced isotropically in the three-body c.m. frame. This has a strong effect on the stopping power, since the particle production in hadron-hadron collisions is forward-backward peaked in the c.m. frame of the colliding particles at high invariant energies.

The effect of three-body collisions can be even better demonstrated by plotting the transverse mass spectra of the produced mesons. Figs. 5 and 6 show the $m_\perp$-spectra of pions, kaons and antikaons at midrapidity produced in central Au+Au collisions at 10.7 A GeV and central Pb+Pb collisions at 40 A GeV. The cascade calculation (i) overestimates the meson yields at midrapidity and also produces too soft $K^+$ $m_\perp$-spectra. Including the RMF into propagation of the baryons (ii) reduces the yields somewhat, but does not change much the slopes. The three-body collisions (iii) make the $m_\perp$-spectra considerably harder. This is again caused by the isotropic emission of the produced mesons in the c.m. frame of the

colliding triple. Applying the in-medium reduced baryon-baryon cross sections (iv) reduces the meson yields without strong changes of the spectra shapes.

The last fact is unexpected, since reducing the cross section should also reduce the interaction volume, where the third particle is looked for, and, hence, reduce the relative fraction of the three-body collisions with respect to two-body collisions. However, this is true only for the baryon-baryon collisions, because we used the in-medium cross sections in this case only. Therefore, the reduction of the number of the three-body collisions of the type baryon-baryon-(baryon or meson) is compensated by the increase of the number of the collisions of the type meson-baryon-(baryon or meson). As a result, the slopes of the $m_\perp$-spectra did not get softer after application of the in-medium baryon-baryon cross sections.

In the case of Au+Au collisions at 10.7 A GeV, the calculation with three-body collisions and vacuum cross sections (iii) provides the best agreement with the experimental transverse mass spectra of $\pi^+$, $K^+$ and $K^-$. For the Pb+Pb system at 40 A GeV, the three-body collisions combined with the in-medium cross sections (iv) produce the best description of the data on $m_\perp$-spectra of $\pi^-$, $K^+$ and $K^-$.

In Fig. 7 we present the inverse slope parameter $T$ of the $K^+$ transverse mass spectrum at midrapidity vs the beam energy. To obtain $T$, following Refs. [48, 49, 50], we fitted the midrapidity transverse mass spectrum by an exponential function:

$$\frac{d^2n}{m_\perp dm_\perp dy} = a \exp\{-m_\perp/T\} \ . \tag{48}$$

Without the three-body collisions, we underpredict the inverse slope parameter $T$ by about 30%. Including the three-body collisions leads to the much better agreement with experiment, except for the points at 5.93 and 7.94 A GeV, where we still underpredict the experimental inverse slope parameter by about 20%.

Fig. 8 shows the midrapidity yields of $\pi^+$, $K^+$, $(\Lambda + \Sigma^0)$ and $K^-$ vs the beam energy for central Au+Au collisions at 1.96, 4.00, 5.93, 7.94, 10.7 A GeV and 20 A GeV and for central Pb+Pb collisions at 30 and 40 A GeV. The corresponding experimental data on pion, kaon, antikaon and hyperon production were taken from Refs. [47, 48, 49, 50, 51, 52, 53, 54, 55]. The calculations for the Au+Au system were done for the impact parameter range $b \leq 3.5$ fm (5% of the geometrical cross section, c.f. [47]). For the Pb+Pb system, we have chosen a slightly larger impact parameter range $b \leq 4$ fm (7% of the geometrical cross section, c.f. [49]).

We observe that the pure cascade calculation (i) overestimates the meson and hyperon production. Using the RMF (ii) reduces the midrapidity meson yields by about 15%. The midrapidity hyperon yield is reduced stronger, by about 30%. This reflects the behaviour of the proton midrapidity yield shown in Fig. 4, since the mean field acts on the hyperons too. The introduction of the three-body collisions (iii) influences the midrapidity yields of the produced particles rather weakly. Finally, the in-medium cross sections (iv) reduce the particle production quite strongly: mesons — by about 30%, and hyperons — by about 50%. As a result the calculation (iv) turns out to be in a good agreement with the data on pion and $K^-$ production, while it underestimates the $K^+$ and hyperon yields below 40 A GeV.

Fig. 9 shows the $K^+/\pi^+$ ratio at midrapidity vs the beam energy. It is interesting, that the three-body collisions reduce the ratio quite strongly. This is due to combination of the two small effects visible in Fig. 8: increase of the pion yield and decrease of the kaon yield by the three-body collisions. The calculation in the RMF mode with vacuum cross sections and three-body collisions (iii) is in the best agreement with the experimental data below 40 A GeV. However, we fail to describe the reduction of the $K^+/\pi^+$ ratio above 30 A GeV.

## IV. SUMMARY AND DISCUSSION

We studied the influence of several many-body effects on particle production in heavy ion collisions at 2-40 A GeV. The calculations were done in the framework of the GiBUU model [7].

First, we implemented the relativistic mean field of the nonlinear Walecka model NL2 [39] in GiBUU. The RMF reduces the stopping power of colliding nuclei and the meson production. In a calculation with RMF, a part of the kinetic c.m. energy of the colliding nuclei transformes into the build-up of the strongly repulsive time component of the $\omega$-field. This leads to less compression and less entropy production by particle-particle collisions. As a consequence, the nuclear matter becomes more transparent when the mean field is taken into account (c.f. Fig. 4). This is an interesting result, since in microscopic transport models the mean field has been usually not taken into account (or switched-off) at high energies (c.f. Refs. [12, 13, 14]).

Second, we implemented the three-body collisions in the model by adopting the geomet-

rical method of Refs. [19, 22, 23, 24] modified to account for the relativistic effects (see Sect.IIC). The three-body collisions increase the inverse slope parameter of the $K^+$ transverse mass spectra to a quite good agreement (within 10%) with experimental data, except for the points at 5.93 and 7.94 A GeV. The additonal transverse momentum is generated due to isotropic emission of the produced particles in the three-body c.m. frame.

The RMF model serves also as a natural base for the construction of in-medium modified baryon-baryon cross sections. Here, we continued a study started in Ref. [14]. Assuming the matrix element of the meson production in a baryon-baryon collision to be not modified by the nuclear medium, we considered the in-medium modifications of phase space and flux factors. We also took into account the in-medium normalization of the Dirac plane wave bispinor. The last effect has led to a strong in-medium reduction of the cross sections. However, the way we extract the in-medium cross sections is very approximate, since it neglects in-medium modifications of the matrix element.

We have also studied the $\pi^+$, $K^+$, $K^-$ and $(\Lambda + \Sigma^0)$-hyperon yields at midrapidity at various beam energies (Fig. 8). Given the ambiguity in the in-medium cross sections, the data are reasonably well described by calculations with the three-body collisions. The same is valid for the $K^+/\pi^+$ ratio at midrapidity plotted vs the beam energy (Fig. 9). However, we do not reproduce the decrease of the $K^+/\pi^+$ ratio above 30 A GeV.

The problems of the microscopic transport models to describe the $K^+/\pi^+$ ratio have usually been ascribed to the excessive pion yield, while the strangeness production was well reproduced overall [12, 13, 14]. This conclusion was based on calculations within the cascade mode using vacuum cross sections. In the present work, by using the in-medium reduced cross sections, we have well reproduced the $\pi^+$ midrapidity yields, while the $K^+$ midrapidity yields are now underpredicted. Since pions represent the major contribution to particle production, we believe that the in-medium cross sections, nevertheless, provide a reasonable base for description of the energy transfer to the inelastic channels. The $K^+$ yield, thus, can be enhanced by more detailed elaboration on the strangeness production channels: $BB \to BYK$ channel below FRITIOF threshold, larger phenomenological strangeness suppression factor $\gamma_s$ at small $\sqrt{s}$ (c.f. Eq.(2)). Moreover, time dependent prehadron cross sections of Ref. [56] could also influence the results on strangeness production. These topics deserve, in our opinion, future studies within the GiBUU or similar transport approaches.

In spite of the fundamental problems with the kinetic theory at high densities, we believe

that our approach combining the baryon propagation in RMF with the in-medium reduced cross sections and three-body collisions provides a realistic description of the HIC dynamics in 10 A GeV domain. It could also serve to model the pre- and after-quark-gluon phase formation stages of a HIC at higher energies.

**Acknowledgments**

We gratefully acknowledge support by the Frankfurt Center for Scientific Computing. We also acknowledge helpful discussions with Dr. T. Gaitanos on the relativistic mean field model. One of us (A.B.L.) is grateful to Prof. I.N. Mishustin and Prof. P. Senger for stimulating discussions and useful comments.

## APPENDIX A: ELASTIC THREE-BODY MATRIX ELEMENT

It is straightforward to write down the three-body elastic collision integral which corresponds to the procedure discussed in Sect. IIC:

$$\begin{aligned} I^{\rm elastic}_{\rm coll,3b}[f^\star_1] \;=\; & \int \frac{g d^3p^\star_2}{(2\pi)^3}\sigma^\star_{12}v^\star_{12}V_{12}\int \frac{g d^3p^\star_3(\gamma_3)_{\rm cm12}}{(2\pi)^3\gamma_3}\,\Phi_3^{-1}(\sqrt{s^\star_{123}}; m^\star_{1'}, m^\star_{2'}, m^\star_{3'}) \\ & \times \int d\Phi_3(p^\star_1+p^\star_2+p^\star_3;\, p^\star_{1'},\, p^\star_{2'},\, p^\star_{3'})\,\sigma^{\star\,-1}_{1'2'}\int d\sigma^\star_{1'2'\to 1''2''} \\ & \times \left(f^\star_{1''}f^\star_{2''}f^\star_{3'}\bar f^\star_1\bar f^\star_2\bar f^\star_3 - f^\star_1 f^\star_2 f^\star_3\bar f^\star_{1''}\bar f^\star_{2''}\bar f^\star_{3'}\right)\,. \end{aligned} \tag{A1}$$

Here $\sigma^\star_{12}$ and $v^\star_{12}$ are, respectively, the total (in-medium) interaction cross section and the relative velocity (Eq.(23)) of 1 and 2;

$$V_{12} = \frac{4}{3}\pi(R_{\rm max})^3\gamma_{12}^{-1} \tag{A2}$$

is the interaction volume, where $R_{\rm max}$ and $\gamma_{12}$ are given by Eqs. (42) and (43), respectively; $\gamma_3 = p^{*0}_3/m^*_3$; $\Phi_3$ and $d\Phi_3$ are the three-body phase space volume (Eq.(37)) and the three-body phase space volume element (Eq.(38)), respectively; $s^\star_{123}\equiv(p^\star_1+p^\star_2+p^\star_3)^2$; $d\sigma^\star_{1'2'\to 1''2''}$ is the elastic differential scattering cross section (Eq.(20)). The quantity

$$\int \frac{g d^3p^\star_3(\gamma_3)_{\rm cm12}}{(2\pi)^3\gamma_3} f^\star_3 \tag{A3}$$

is the density of particles in the c.m. frame of the particles 1 and 2.

Notice, that Eq.(A1) takes into account the two transitions: $123 \to 1'2'3'$ by the microcanonical sampling the kinetic momenta of $1', 2'$ and $3'$ according to Eq.(44), and the elastic scattering $1'2' \to 1''2''$ afterwards. The divisions by $\Phi_3$ and by $\sigma^\star_{1'2'}$ are done in Eq.(A1) in order to normalize the total transition probabilities to the unity and to the branching ratio of the elastic channel $\sigma^{\rm elastic\,\star}_{1'2'}/\sigma^\star_{12}$, respectively. Here $\sigma^{\rm elastic\,\star}_{1'2'} = \int d\sigma^\star_{1'2'\to 1''2''}$.

Subsututing the explicit expressions for $d\Phi_3(p^\star_1 + p^\star_2 + p^\star_3;\, p^\star_{1'},\, p^\star_{2'},\, p^\star_{3'})$ and for $d\sigma^\star_{1'2'\to 1''2''}$ obtained, respectively, from Eqs. (38) and (20) into Eq.(A1) and changing the order of integrations, one can transform Eq.(A1) to the form of Eq.(17):

$$
\begin{aligned}
I^{\rm elastic}_{\rm coll,3b}[f^\star_1] \;=\; & \int \frac{g d^3p^\star_2}{(2\pi)^3}\sigma^\star_{12} v^\star_{12} V_{12} \int \frac{g d^3p^\star_3 (\gamma_3)_{\rm cm12}}{(2\pi)^3\gamma_3}\,\Phi_3^{-1}(\sqrt{s^\star_{123}}; m^\star_{1'}, m^\star_{2'}, m^\star_{3'}) \\
& \times \int \frac{d^3p^\star_{1'}}{(2\pi)^3 2p^{\star 0}_{1'}} \int \frac{d^3p^\star_{2'}}{(2\pi)^3 2p^{\star 0}_{2'}} \int \frac{d^3p^\star_{3'}}{(2\pi)^3 2p^{\star 0}_{3'}} \delta^{(4)}(p^\star_1 + p^\star_2 + p^\star_3 - p^\star_{1'} - p^\star_{2'} - p^\star_{3'}) \\
& \times \sigma^{\star\,-1}_{1'2'}\,\sigma^{\rm elastic\,\star}_{1'2'}\,(f^\star_{1'} f^\star_{2'} f^\star_{3'} \bar f^\star_1 \bar f^\star_2 \bar f^\star_3 - f^\star_1 f^\star_2 f^\star_3 \bar f^\star_{1'} \bar f^\star_{2'} \bar f^\star_{3'})\;. \qquad \text{(A4)}
\end{aligned}
$$

In derivation of Eq.(A4), we used the relations

$$\sigma^\star_{1'2'} \;=\; \sigma^\star_{1''2''}\;, \qquad \text{(A5)}$$

$$I^\star_{1'2'} \;=\; I^\star_{1''2''}\;, \qquad \text{(A6)}$$

valid for the elastic scattering $1'2' \to 1''2''$ and the detailed balance formula

$$\overline{|M|^2_{1'2'\to 1''2''}} = \overline{|M|^2_{1''2''\to 1'2'}}\;. \qquad \text{(A7)}$$

Finally, we have also changed the notations as $1'' \to 1'$ and $2'' \to 2'$. By putting all the $\gamma$-factors equal to unity and also neglecting the Pauli blocking of the final states, the loss term of Eq.(A4) is reduced to the loss term of Eq.(4.17) from Ref. [24]. The comparison of the gain term of our Eq.(A4) to the gain term of Eq.(4.17) from Ref. [24] is not straightforward, since we used an assumption of the microcanonical sampling of the particles $1'$, $2'$ and $3'$ momenta, which has not been used in Ref. [24].

By comparison Eqs. (A4) and (17) we get the following expression for the invariant matrix element of the elastic three-body collisions:

$$\overline{|M|^2_{123\to 1'2'3'}} \;=\; \frac{3!\,2!\,\sigma^\star_{12}\,I^\star_{12}\,\frac{4}{3}\pi (R_{\rm max})^3 (\gamma_3)_{\rm cm12}}{m^\star_1 m^\star_2 m^\star_{1'} m^\star_{2'} m^\star_{3'} (2g)^3 (2\pi)^4 \gamma_{12}} \Phi_3^{-1}(\sqrt{s^\star_{123}}; m^\star_{1'}, m^\star_{2'}, m^\star_{3'}) \frac{\sigma^{\rm elastic\,\star}_{1'2'}}{\sigma^\star_{1'2'}}\;. \qquad \text{(A8)}$$

The ratio of the $\gamma$-factors in the c.m. frame of 1 and 2 can be rewritten in the explicitly covariant form as

$$\frac{(\gamma_3)_{\rm cm12}}{\gamma_{12}} = \frac{2 m^\star_1\, m^\star_2\, p^\star_3\, (p^\star_1 + p^\star_2)}{m^\star_3\,(m^\star_2\, p^\star_1 + m^\star_1\, p^\star_2)(p^\star_1 + p^\star_2)}\;. \qquad \text{(A9)}$$

[1] G.F. Bertsch and S. Das Gupta, Phys. Rep. **160**, 189 (1988).

[2] W. Cassing, V. Metag, U. Mosel and K. Niita, Phys. Rep. **188**, 363 (1990).

[3] S. Teis, W. Cassing, M. Effenberger, A. Hombach, U. Mosel and Gy. Wolf, Z. Phys. A **356**, 421 (1997).

[4] W. Cassing and E.L. Bratkovskaya, Phys. Rep. **308**, 65 (1999).

[5] M. Effenberger, E.L. Bratkovskaya, and U. Mosel, Phys. Rev. C **60**, 44614 (1999).

[6] M. Effenberger, PhD thesis, Uni. Giessen, 1999, http://theorie.physik.uni-giessen.de/html/dissertations.html

[7] http://theorie.physik.uni-giessen.de/GiBUU

[8] A.B. Larionov, W. Cassing, C. Greiner, U. Mosel, Phys. Rev. C **62**, 064611 (2000).

[9] A.B. Larionov and U. Mosel, Nucl. Phys. A **728**, 135 (2003).

[10] E.E. Kolomeitsev et al., J. Phys. G **31**, S741 (2005).

[11] A.B. Larionov and U. Mosel, Phys. Rev. C **72**, 014901 (2005).

[12] H. Weber et al., Phys. Rev. C **67**, 014904 (2003).

[13] E.L. Bratkovskaya et al., Phys. Rev. Lett. **92**, 032302 (2004).

[14] M. Wagner, A.B. Larionov, and U. Mosel, Phys. Rev. C **71**, 034910 (2005).

[15] Yu.B. Ivanov and V.N. Russkikh, nucl-th/0607070

[16] I.C. Arsene et al., Phys. Rev. C **75**, 034902 (2007).

[17] http://www.gsi.de/fair

[18] E. Lifshitz and L. Pitaevskii, *Physical Kinetics* (Pergamon, New York, 1981).

[19] St. Mrówczyński, Phys. Rev. C **32**, 1784 (1985).

[20] A.B. Larionov, K. Gallmeister, U. Mosel, GSI Scientific Report 2005, p. 255, http://www.gsi.de/library/GSI-Report-2006-1

[21] T. Kodama, S.B. Duarte, K.C. Chung, R.A.M.S. Nazareth, Phys. Rev. Lett. **49**, 536 (1982).

[22] G. Batko, J. Randrup, T. Vetter, Nucl. Phys. A **536**, 786 (1992); ibid. **546**, 761 (1992).

[23] A. Bonasera and T. Maruyama, Prog. Theor. Phys. **90**, 1155 (1993).

[24] A. Bonasera, F. Gulminelly, J. Molitoris, Phys. Rep. **243**, 1 (1994).

[25] Z.-S. Wang, Y.-K. Ho, Phys. Rev. C **51**, 182 (1995).

[26] P. Daniewlewicz, Nucl. Phys. A 673, 375 (2000).

[27] B. ter Haar and R. Malfliet, Phys. Rev. C **36**, 1611 (1987).

[28] C. Fuchs, A. Faessler, and M. El-Shabshiri, Phys. Rev. C **64**, 024003 (2001).

[29] L.D. Landau, JETP **30**, 1058 (1956) (Sov. Phys. JETP **3**, 920); JETP **32**, 59 (1957) (Sov. Phys. JETP **5**, 101).

[30] I.Ia. Pomeranchuk, JETP **35**, 524 (1958) (Sov. Phys. JETP **8**, 361).

[31] J. Geiss, W. Cassing, and C. Greiner, Nucl. Phys. A **644**, 107 (1998).

[32] T. Falter, W. Cassing, K. Gallmeister, and U. Mosel, Phys. Rev. C **70**, 054609 (2004).

[33] G.M. Welke, M. Prakash, T.T.S. Kuo, and S. Das Gupta, Phys. Rev. C **38**, 2101 (1988).

[34] B. Blättel, V. Koch and U. Mosel, Rep. Prog. Phys. **56**, 1 (1993).

[35] T. Klähn et al., Phys. Rev. C **74**, 035802 (2006).

[36] G.A. Lalazissis, J. König, and P. Ring, Phys. Rev. C **55**, 540 (1997).

[37] J.D. Bjorken and S.D. Drell, *Relativistic quantum mechanics*, McGraw-Hill, New York, 1965.

[38] V.R. Pandharipande, S.C. Pieper, Phys. Rev. C **45**, 791 (1992).

[39] A. Lang, W. Cassing, U. Mosel and K. Weber, Nucl. Phys. A **541**, 507 (1992).

[40] We would like to remind that we are using the notations of Ref. [36] for the RMF parameters. In order to go back to the notations of Ref. [39], one needs to do the following replacements in the Lagrangian density (3): $g_\sigma \to g_s$, $g_\omega \to g_v$, $m_\sigma \to m_s$, $m_\omega \to m_v$, $g_2 \to -B$, $\sigma \to -\sigma$ and $g_3 \to C$.

[41] K. Hagiwara et al., Phys. Rev. D **66**, 010001 (2002).

[42] Except for the case of $3 \to 2$ collisions, where the matrix element can be obtained by using the detailed balance relations from the cross section of the inverse process.

[43] K.A. Bugaev, M.I. Gorenstein, H. Stöcker and W. Greiner, Phys. Lett. B **485**, 121 (2000).

[44] K.A. Bugaev, arXiv:nucl-th/0611102.

[45] B.B. Back et al., Phys. Rev. C **66**, 054901 (2002).

[46] T. Anticic et al., Phys. Rev. C **69**, 024902 (2004).

[47] L. Ahle et al., Phys. Lett. B **476**, 1 (2000).

[48] L. Ahle et al., Phys. Lett. B **490**, 53 (2000).

[49] S. Afanasiev et al., Phys. Rev. C **66**, 054902 (2002).

[50] V. Friese, J. Phys. G **30**, 119 (2004).

[51] A. Mischke et al., J. Phys. G **28**, 1761 (2002).

[52] A. Mischke et al., Nucl. Phys. A **715**, 453 (2003).

[53] S. Ahmad et al., Phys. Lett. B **382**, 35 (1996).

[54] C. Pinkenburg, Nucl. Phys. A **698**, 495 (2002).

[55] F. Antinori, Nucl. Phys. A **661**, 130 (1999).

[56] K. Gallmeister and U. Mosel, nucl-th/0701064.

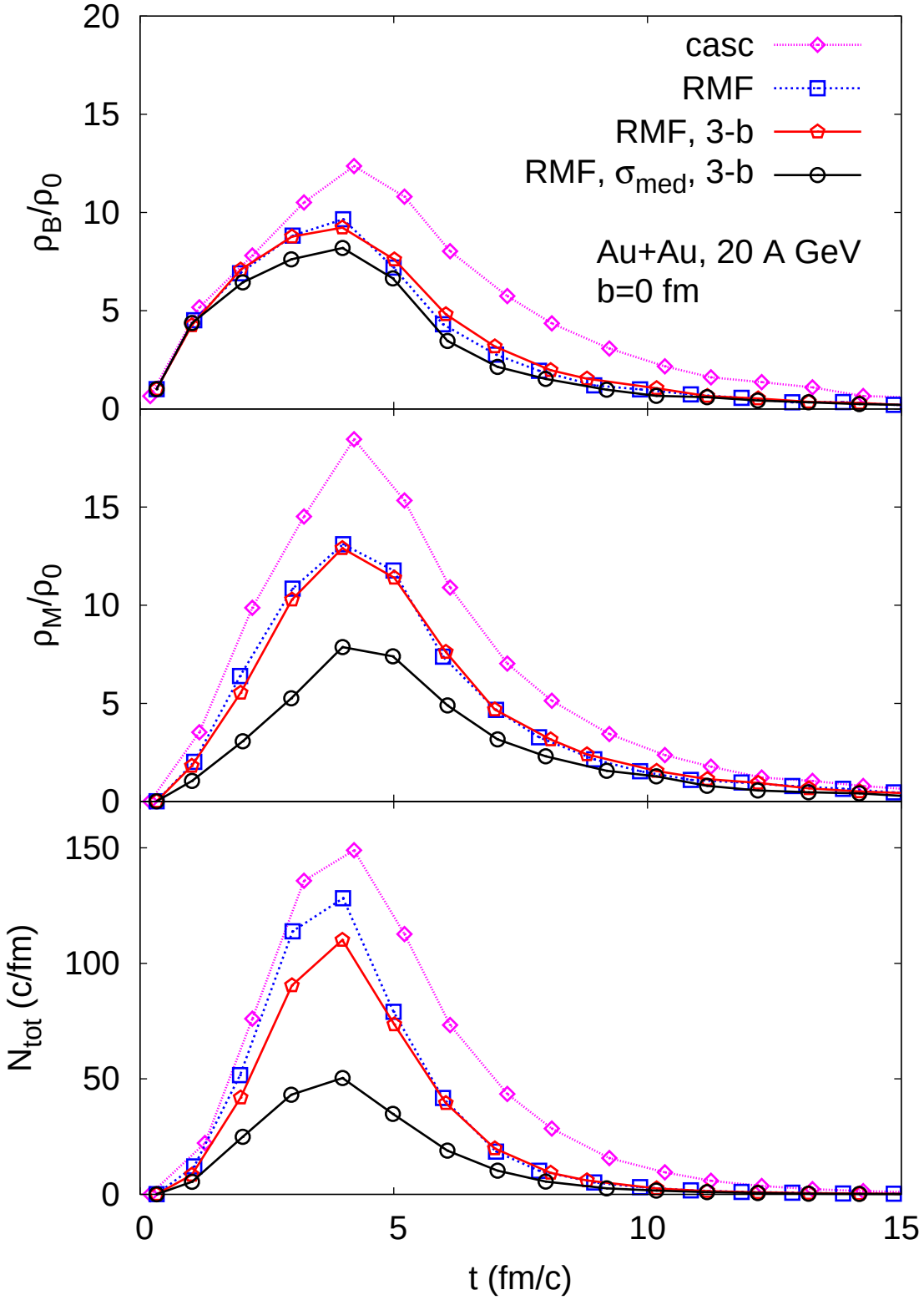


FIG. 1: (color online) Time evolution of the central baryon density (top panel), of the central meson density (middle panel) and of the total collision frequency (bottom panel) for central Au+Au collision at 20 A GeV. Binary cascade calculation is represented by dotted lines with open rombuses. RMF calculation including binary collisions only and vacuum cross sections is shown by dashed lines with open boxes. Results with RMF including also the three-body collisions with vacuum cross sections are plotted by solid lines with open pentagons. RMF calculation with the three-body collisions and in-medium cross sections is shown by solid lines with open circles.

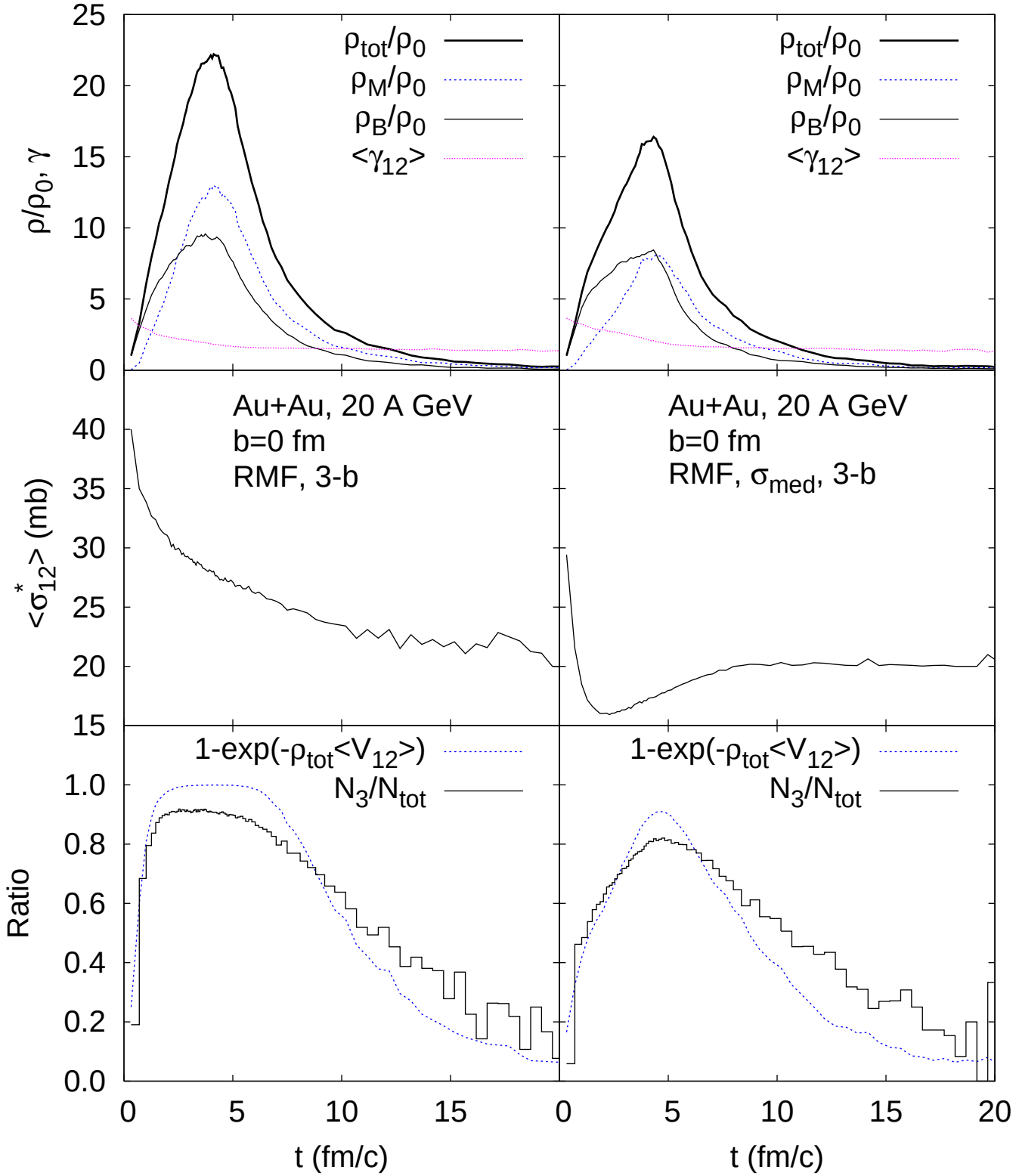


FIG. 2: (color online) Top panels: time dependence of the total (baryon plus meson) density — thick solid lines, meson density — dashed lines, baryon density — thin solid lines and of the $\gamma$-factor (Eq.(43)) averaged over colliding pairs — dotted lines. Middle panels: cross section used in calculation of the radius $R_{\max}$ (Eq.(42)) averaged over colliding pairs. Bottom panels: the ratio of the three-body and the total (two- plus three-body) collision freequencies — solid histograms and the estimate of Eq.(47) — dashed lines. The calculations are done with RMF including three-body collisions. Left column: with vacuum cross sections. Right column: with in-medium cross sections.

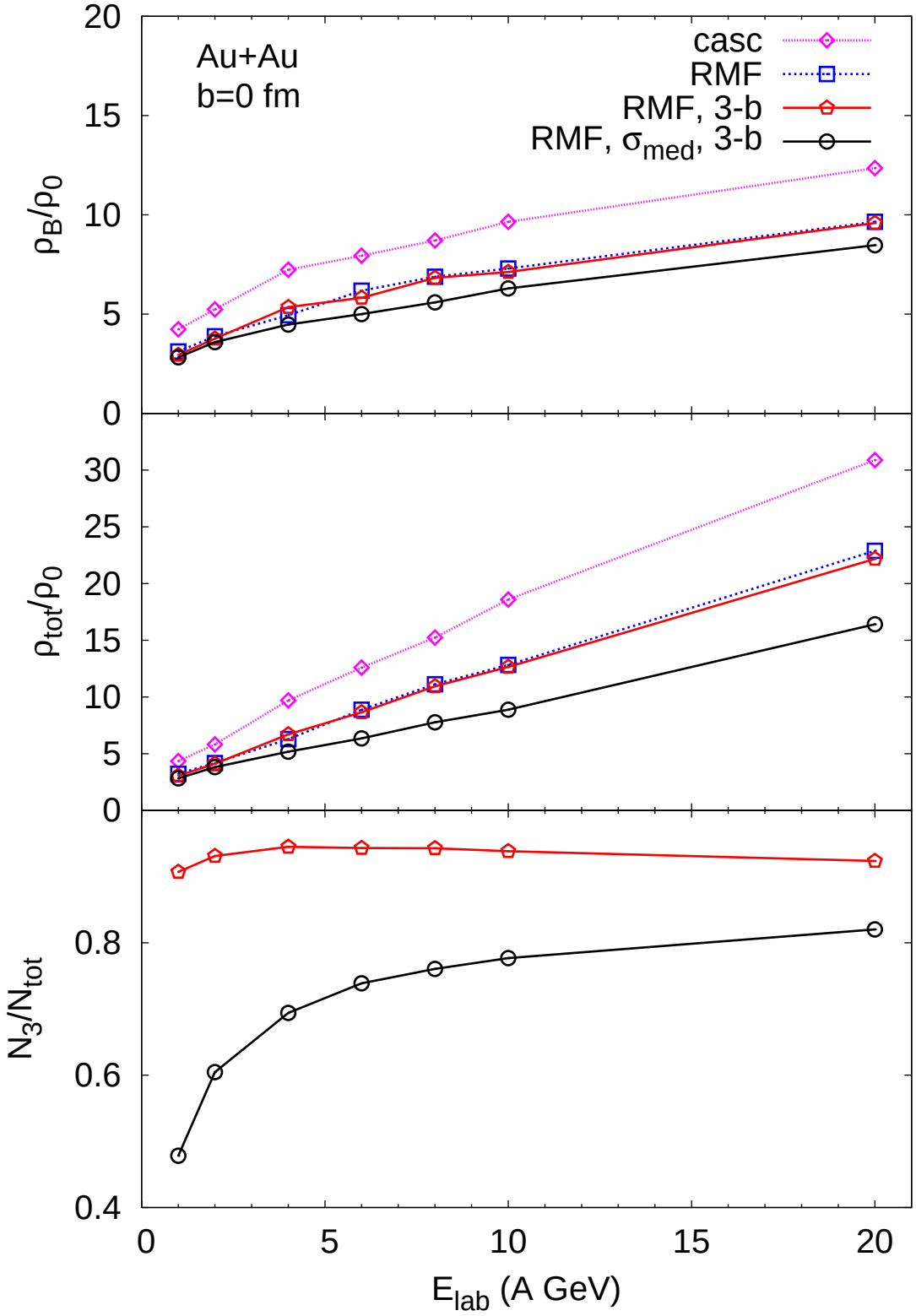


FIG. 3: (color online) Top, middle and bottom panels, respectively: the maximum central baryon density, the maximum central total (i.e. baryon plus meson) density and the maximum ratio of the three-body collision frequency to the total (two- plus three-body) collision frequency reached in the central Au+Au collision vs the beam energy. Various calculations are shown with the same notations as in Fig. 1.

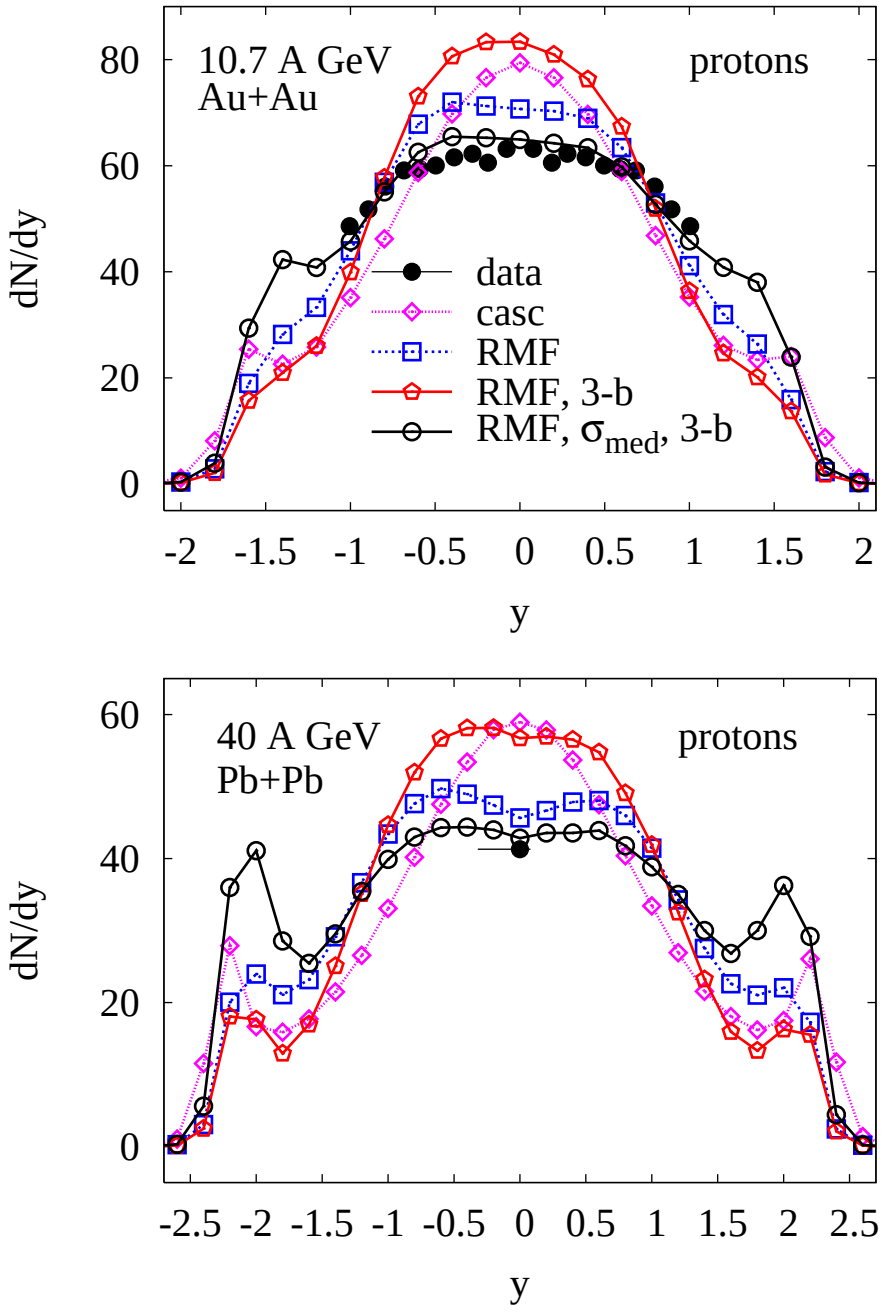


FIG. 4: (color online) Proton rapidity disributions for central ($b \leq 3.5$ fm) Au+Au collisions at 10.7 A GeV (upper panel), and central ($b \leq 4$ fm) Pb+Pb collisions at 40 A GeV (lower panel). The experimental data for the Au+Au system are taken from Ref. [45] and correspond to 5% most central events. The data for Pb+Pb are from Ref. [46] (7% centrality). Notations are the same as in Fig. 1.

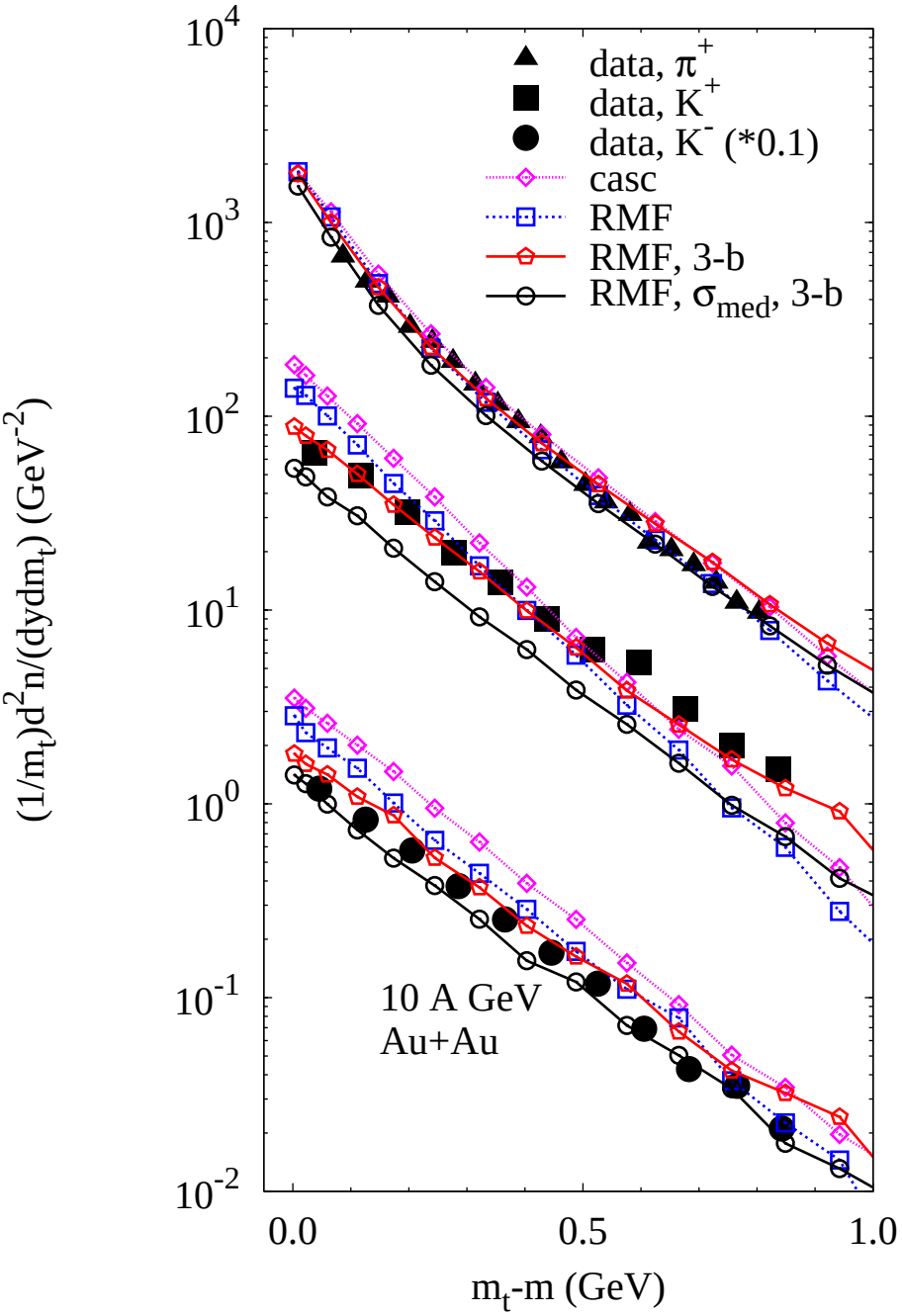


FIG. 5: (color online) $\pi^+$, $K^+$ and $K^-$ transverse mass spectra at midrapidity from central ($b \leq 3.5$ fm) Au+Au collisions at 10.7 A GeV. The rapidity region is $|(y - y_{NN})/y_{NN}| < 0.125$, where $y_{NN}$ is the c.m. rapidity in the laboratory frame. The $K^-$ spectra are multiplied by 0.1. The data are from Refs. [47, 48]. Notations are the same as in Fig. 1.

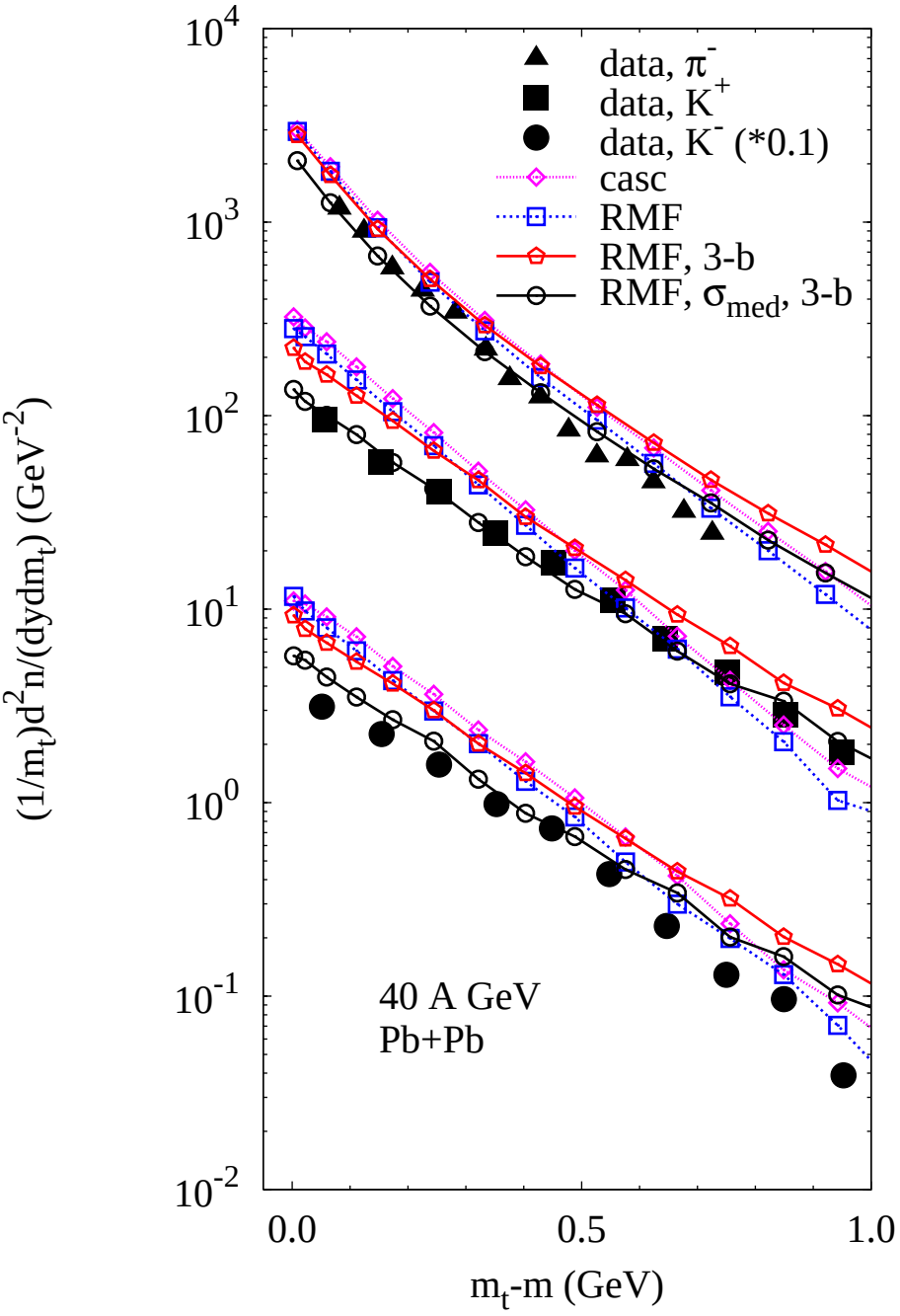


FIG. 6: (color online) $\pi^-$, $K^+$ and $K^-$ transverse mass spectra at midrapidity from central ($b \leq 4$ fm) Pb+Pb collisions at 40 A GeV. The rapidity region is $|y-y_{NN}| < 0.2$ for $\pi^-$ and $|y-y_{NN}| < 0.1$ for $K^{\pm}$. The $K^-$ spectra are multiplied by 0.1. The data are from Ref. [49]. Notations are the same as in Fig. 1.

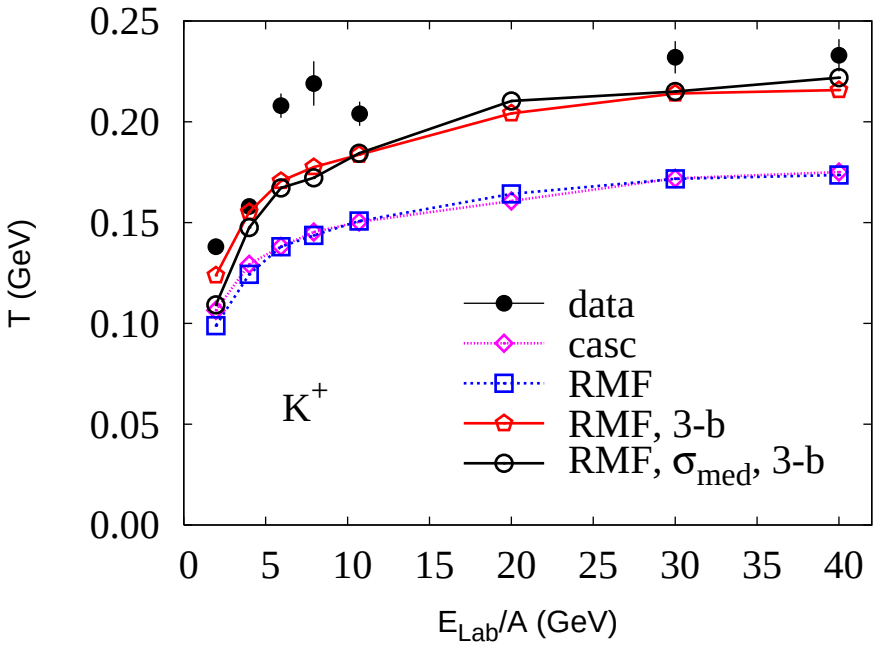


FIG. 7: (color online) Inverse slope parameter of the $K^+$ transverse mass spectrum at midrapidity for central collisions of Au+Au and Pb+Pb as function of the beam energy. Data from Refs. [48, 49, 50]. Notations are the same as in Fig. 1.

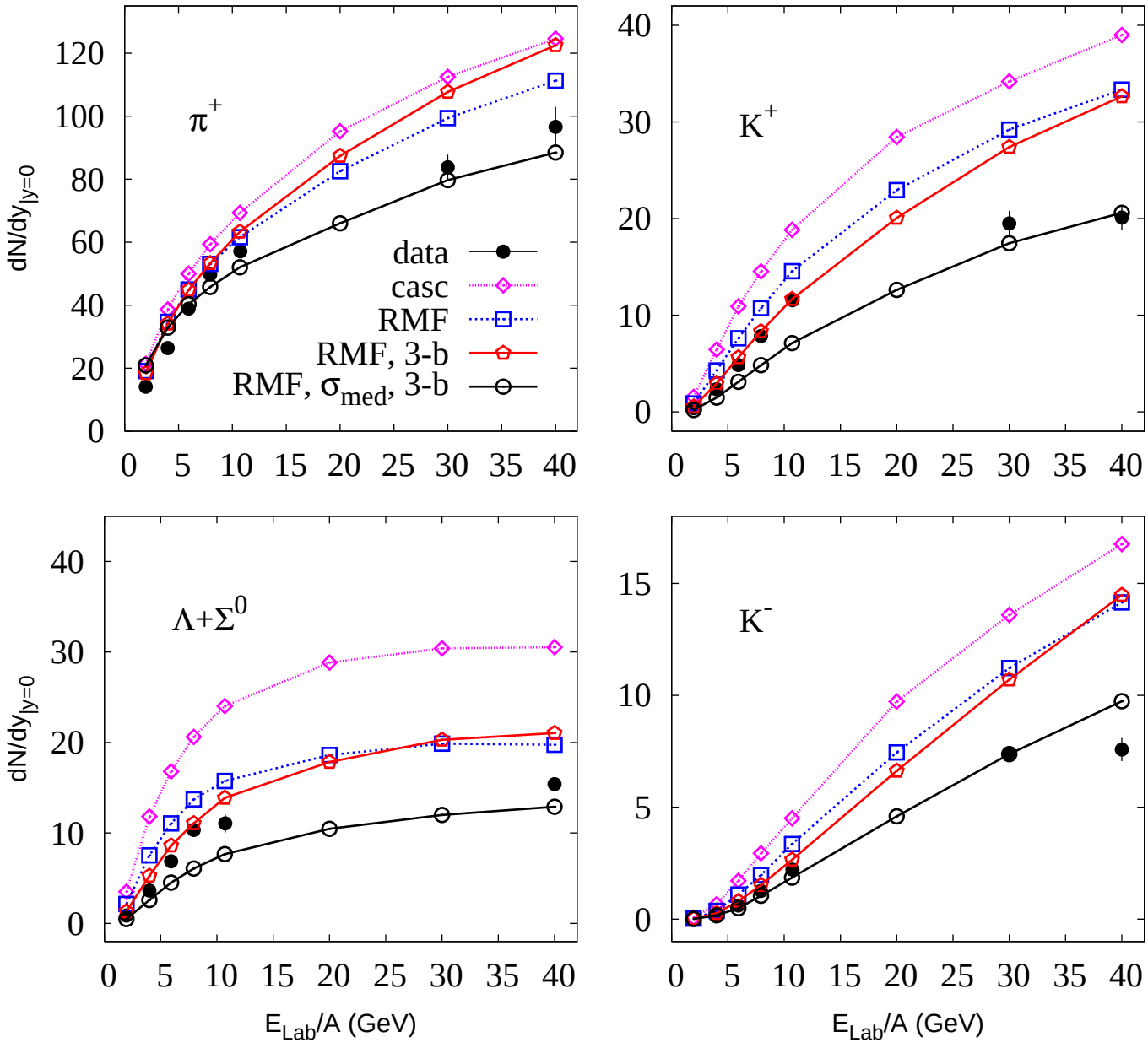


FIG. 8: (color online) The yield of $\pi^+$ (upper left panel), $K^+$ (upper right panel), $\Lambda + \Sigma^0$ (lower left panel) and $K^-$ (lower right panel) at midrapidity as function of the beam energy for central collisions of Au+Au at $E_{lab} \leq 20$ A GeV and Pb+Pb at $E_{lab} = 30$ and 40 A GeV. The data are from Refs. [47, 48, 49, 50, 51, 52, 53, 54, 55]. Notations are the same as in Fig. 1.

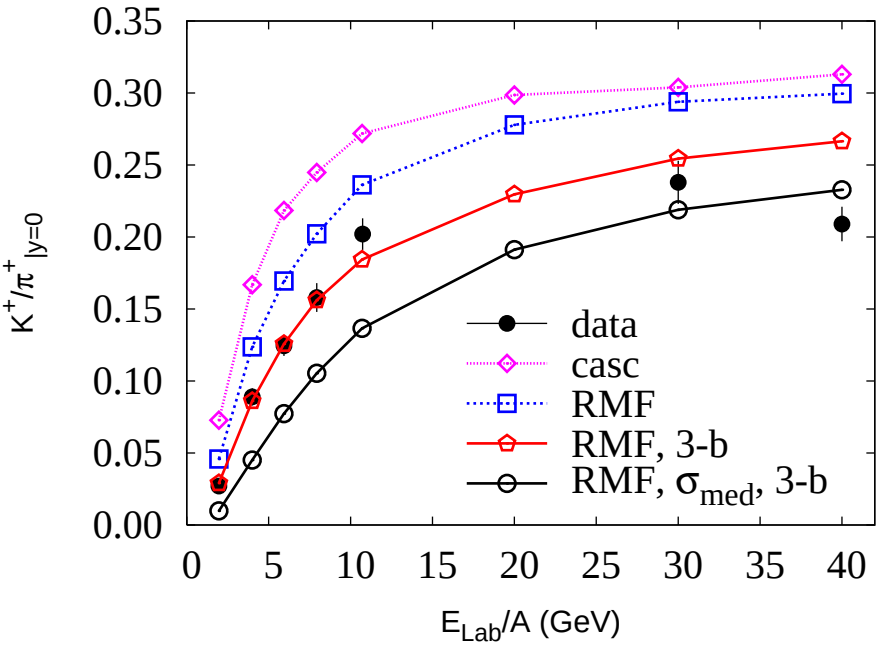


FIG. 9: (color online) The ratio of the midrapidity yields $K^+/\pi^+$ for central Au+Au and Pb+Pb collisions. The data are from [47, 49, 50]. Notations are the same as in Fig. 1.